EARTHQUAKE ENGINEERING AND STRUCTURAL DYNAMICS, VOL. 27, 15–28 (1998)

SEISMIC RESPONSE OF MULTI-LAYERED BASINS WITH VELOCITY GRADIENTS UPON INCIDENCE OF PLANE SHEAR WAVES

YONG ZENG[1]* AND RAFAEL BENITES[2]
[1] *QUAKES, Department of Earthsciences, University of Queensland, QLD4072, Australia*
[2] *Institute of Geological & Nuclear Sciences, PO Box 1320, Wellington, New Zealand*

SUMMARY

A boundary integral scheme based on boundary-integral discrete-wave-number approach has been developed to compute the seismic response of two-dimensional irregular-shaped basins with horizontal soil layers. Each layer exhibits a linear gradient of shear wave velocity with depth. The approach combines the boundary-integral representation of the seismic wave field outside the basin with plane wave representation of the seismic wave field inside the basin. The propagation throughout the layers is performed by matrix propagators in which the effect of the vertical variation of the velocity is incorporated by using confluent hyper-geometric functions of the Whittaker type. Our method is tested against other well-accepted solutions for the case of a circular basin with excellent agreement. Test of the ground response for a semi-circular basin with radius a shows that stable solutions are obtained if the chosen model parameters satisfy following conditions:

(1) the distance from the sources to the interface is greater than $0{\cdot}1a$;
(2) the distance between the sources is smaller than a quarter of the incident wavelength; and
(3) the discrete wave-number step is smaller than $2\pi/4a$.

The computation of ground response of basins with a sharp interface and several horizontal deposits leads to the following main results: (1) the amplification of a basin with velocity gradients is larger than that of a basin with homogeneous layers; (2) the frequencies of the second- and third-order harmonics for a basin with velocity gradients are lower than those of a basin with homogeneous layers; and (3) the response amplitude of the basin with velocity gradients attenuates more slowly in time domain than when layers are homogeneous.

Since these results have been obtained for realistic values of basin geometrical and mechanical consideration, they should find some interest in earthquake engineering or seismic microzonation studies. © 1998 John Wiley & Sons, Ltd.

Earthquake Engng. Struct. Dyn., **27**, 15–28 (1998)

KEY WORDS: SH waves; seismic modelling; basins; velocity gradient

INTRODUCTION

The seismic response of sedimentary deposits in basins exhibiting lateral irregularities has been studied by many authors, both experimentally and theoretically (see a review by Aki[1]). The present study pertains to the theoretical methods that treat two-dimensional basins with complex geometrical and material properties. With the exception of the finite difference method, which directly solves the wave equation at time steps

* Correspondence to: Yong Zeng, QUAKES, Department of Earth Sciences, The University of Queensland, St. Lucia, Brisbane, QLD 4072, Australia

Contract grant sponsor: Institute of Geological and Nuclear Sciences
Contract grant sponsor: Joint New Zealand-Sino Scientific Research Program

CCC 0098–8847/98/010015–14$17·50

Received 7 December 1995
Revised 16 December 1996

throughout computational spatial meshes, most analytical and numerical methods owe their versatility to the ways in which the seismic wave field has been represented and the boundary conditions treated for a particular problem. For example, Trifunac[2] found a closed-form solution for the anti-plane motion (SH wave) of a semi-cylindrical basin upon the incidence of plane harmonic waves. The wave field representations that are particularly relevant to the technique presented here are: the superposition of plane harmonic waves with unknown strengths and the indirect boundary integral.

The first representation was proposed by Aki and Larner[3] to study simple cosine-shaped basins, and extended to more complex structures by Bouchon[4] and Bard and Bouchon.[5] The computational schemes developed by these authors are in the wave-number domain assuming spatial periodicity of the structure in which the strength of each plane wave is determined by satisfying the boundary conditions. Furthermore, Bard and Tucker[6] and Bard and Gariel[7] combine Aki–Larner technique with the confluent hyper-geometric function of Whittaker type or combine Aki–Larner technique with Thomson–Haskell matrix propagators to investigate the response of 2-D valleys with large velocity gradients. However, results are accurate only when the slopes involved in the structure are gentle in comparison with the wavelengths considered, because the forward scattered and diffracted waves are not well represented by travelling plane waves (the so-called Rayleigh ansatz error).

The second representation, using the indirect boundary integral, is based upon a point wave source distribution along the boundaries of the structure, in which the strength of each source is determined by satisfying the boundary conditions globally. This method is particularly suited for sharp boundaries, regardless of the incident wavelengths and has been extensively used in basin and topography response studies.[4,8–12] The numerical schemes adopted in these studies differ only in the type of Green's function used and in the way boundary conditions are satisfied. Furthermore, the boundary integral method has been extended to two- and half-dimensional cases[13,14] and three-dimensional cases.[15–18]

An attempt to combine both representation into a hybrid approach is due to Bravo *et al.*[19] to study semi-cylindrical basins filled with horizontal homogeneous layers of sediments. The transfer functions from bottom of the basin to free surface are computed using Thomson–Haskell propagators, and the wave field outside the basin using distribution of point wave sources at regular intervals. The strengths of the point sources are determined from satisfying the boundary conditions in a least-squares sense. This approach is capable of avoiding Rayleigh ansatz error (due to sharp interfaces of basins). The stability of the numerical approach has not been discussed previously in the literature.

Our approach extends Bravo *et al.*'s boundary-integral discrete-wave-number method by incorporating: arbitrary shaped basin-bedrock interfaces, multi-layered deposits, and linear velocity gradients in each layer. The first two are made possible by Bravo *et al.*'s boundary-integral discrete-wave-number method and the third by using the solution of the wave equation based on confluent hyper-geometrical functions of the Whittaker type (see References 6, 7, 20 and 21). Our approach combines the advantage of Bravo *et al.*'s and that of Bard *et al.*'s, i.e., (1) it accurately models scattered waves of a basin with a sharp interface; (2) it yields an accurate solution of the wave field in a layer with a velocity gradient instead of an approximate solution obtained by modelling finely layered media. Consequently, the wave field inside the basin is presented by propagators of the multi-layers with velocity gradients instead of propagators of homogeneous layers or a solution of the wave field in one single layer with a velocity gradient. Furthermore, the stability of the approach is investigated. The results obtained from supposed basins should have, in our opinion, some interest for earthquake engineering or seismic microzonation studies.

FORMULATION OF THE METHOD

An irregular two-dimensional basin with flat layers embedded in a homogeneous elastic half-space is illustrated in Figure 1. Each layer exhibits a vertical gradient of shear wave velocity. Using the boundary integral scheme described by Sanchez-Sesma and Rosenblueth,[9] the scattered wave field in the half-space can be represented by adding up the wave contributions of N artificial sources regularly distributed along $\xi(x)$. The total wave

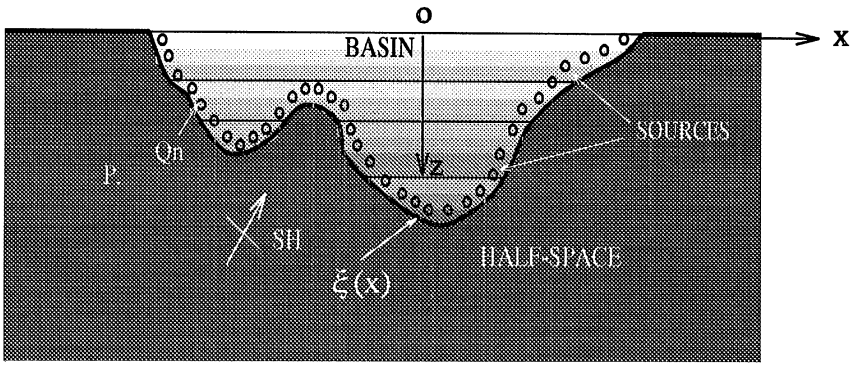

Figure 1. A multi-layered basin with velocity gradients embedded in a half-space

field u_E in the half-space can be written as

$$u_E(P) = u_0(P) + \sum_{n=1}^{N} A_n G(P, Q_n) \tag{1}$$

where $u_0(P)$ is the incident wave field measured at an arbitrary point P in the half-space; $G(P, Q_n)$ represents the Green's function at P due to a source at point Q_n of $\xi(x)$; and A_n is a complex number that represents the strength of the contribution of each source.

A plane wave representation and matrix propagators are used to specify the wave field inside the basin. The incorporation of the vertical velocity gradient is made possible by solving the corresponding wave equation in unbounded media, which yields a closed-form solution in terms of confluent hyper-geometric functions. This solution is due to Whittaker.[20,21] The solution of the propagating wave equation of an SH wave in an inhomogeneous layer $p+1$ for a discrete horizontal wave number k_m is expressed as

$$u^{(p+1)}(x,z,t) = [A^{(p+1)} W_1^{(p+1)}(z - z_{p+1}) + B^{(p+1)} W_2^{(p+1)}(z - z_{p+1})]\mathrm{e}^{\omega t - \mathrm{i} k_m x} \tag{2}$$

where $u^{(p+1)}(x,z,t)$ is displacement in a co-ordinate system $x-z$ at the time t; $A^{(p+1)}$ and $B^{(p+1)}$ are unknown complex coefficients; ω is angular frequency; and $W_1^{(p+1)}(z - z_{p+1})$ and $W_2^{(p+1)}(z - z_{p+1})$ are hyper-geometric functions of Whittaker type associated with waves travelling up and down, respectively (The functions of Whittaker type are expressed explicitly in Bard and Tucker's paper[6]). The value of z_{p+1} represents the depth of the top of layer $p+1$.

The displacement and traction at the interface between the horizontal layers p and $p+1$ satisfy the conditions of continuity:

$$u^{(p)}(z_{p+1} - z_p) = u^{(p+1)}(z_{p+1} - z_{p+1}) \tag{3}$$

$$\mu^{(p)}(z_{p+1} - z_p)\frac{\mathrm{d}u^{(p)}}{\mathrm{d}z}(z_{p+1} - z_p) = \mu^{(p+1)}(z_{p+1} - z_{p+1})\frac{\mathrm{d}u^{(p+1)}}{\mathrm{d}z}(z_{p+1} - z_{p+1}) \tag{4}$$

where $\mu^{(p)}(z_{p+1} - z_p)$ and $\mu^{(p+1)}(z_{p+1} - z_{p+1})$ are rigidities at the bottom of layer p and at the top of layer $p+1$.

Substituting equation (2) into equations (3) and (4), we obtain the propagators matrix (similar to the Thomson–Haskell propagators) from the top layer (i.e. layer 1) to layer $p+1$:

$$\begin{pmatrix} A^{(p+1)} \\ B^{(p+1)} \end{pmatrix} = \begin{pmatrix} f_{11}^{(p)} & f_{12}^{(p)} \\ f_{21}^{(p)} & f_{22}^{(p)} \end{pmatrix} \begin{pmatrix} f_{11}^{(p-1)} & f_{12}^{(p-1)} \\ f_{21}^{(p-1)} & f_{22}^{(p-1)} \end{pmatrix} \cdots \begin{pmatrix} f_{11}^{(1)} & f_{12}^{(1)} \\ f_{21}^{(1)} & f_{22}^{(1)} \end{pmatrix} \begin{pmatrix} A^{(1)} \\ B^{(1)} \end{pmatrix} \tag{5}$$

where

$$f_{11}^{(p)} = \frac{W_1^{(p)}(z_{p+1}-z_p)D_2 - \mu W_2^{(p+1)}(0)D_3}{W_1^{(p+1)}(0)D_2 - W_2^{(p+1)}(0)D_1}$$

$$f_{12}^{(p)} = \frac{W_2^{(p)}(z_{p+1}-z_p)D_2 - \mu W_2^{(p+1)}(0)D_4}{W_1^{(p+1)}(0)D_2 - W_2^{(p+1)}(0)D_1}$$

$$f_{21}^{(p)} = \frac{W_1^{(p)}(z_{p+1}-z_p)D_1 - \mu W_1^{(p+1)}(0)D_3}{W_2^{(p+1)}(0)D_1 - W_1^{(p+1)}(0)D_2}$$

$$f_{22}^{(p)} = \frac{W_2^{(p)}(z_{p+1}-z_p)D_1 - \mu W_1^{(p+1)}(0)D_4}{W_2^{(p+1)}(0)D_1 - W_1^{(p+1)}(0)D_2}$$

$$D_1 = \mathrm{d}W_1^{(p+1)}(0)/\mathrm{d}z$$

$$D_2 = \mathrm{d}W_2^{(p+1)}(0)/\mathrm{d}z$$

$$D_3 = \mathrm{d}W_1^{(p)}(z_{p+1}-z_p)/\mathrm{d}z$$

$$D_4 = \mathrm{d}W_2^{(p)}(z_{p+1}-z_p)/\mathrm{d}z$$

and $\mu = \mu^{(p)}(z_{p+1}-z_p)/\mu^{(p+1)}(0)$.

Equation (5) can be simplified using the following notation:

$$\begin{pmatrix} f_{11}^{(p)} & f_{12}^{(p)} \\ f_{21}^{(p)} & f_{22}^{(p)} \end{pmatrix} \begin{pmatrix} f_{11}^{(p-1)} & f_{12}^{(p-1)} \\ f_{21}^{(p-1)} & f_{22}^{(p-1)} \end{pmatrix} \cdots \begin{pmatrix} f_{11}^{(1)} & f_{12}^{(1)} \\ f_{21}^{(1)} & f_{22}^{(1)} \end{pmatrix} = \begin{pmatrix} f_{11} & f_{12} \\ f_{21} & f_{22} \end{pmatrix} \tag{6}$$

so that equation (5) can be written as

$$\begin{pmatrix} A^{(p+1)} \\ B^{(p+1)} \end{pmatrix} = \begin{pmatrix} f_{11} & f_{12} \\ f_{21} & f_{22} \end{pmatrix} \begin{pmatrix} A^{(1)} \\ B^{(1)} \end{pmatrix} \tag{7}$$

$A^{(1)}$ and $B^{(1)}$ in equation (7) have the relation:

$$A^{(1)} = \alpha B^{(1)} \tag{8}$$

where

$$\alpha = \frac{-\mathrm{d}W_2^{(1)}(0)/\mathrm{d}z}{\mathrm{d}W_1^{(1)}(0)/\mathrm{d}z}$$

determined by the free-surface boundary condition $[\mathrm{d}u^{(1)}(0)]/\mathrm{d}z = 0$.

Substituting equations (7) and (8) into equation (2) gives the total displacement field due to M discrete wave numbers as

$$u^{(p+1)}(x,z,t) = \sum_{m=-M}^{M} B_m^{(1)} l_m(x, z-z_{p+1}, t) \tag{9}$$

where $l_m(x,z-z_{p+1},t) = [(f_{11}\alpha + f_{12})W_1^{(p+1)}(z-z_{p+1}) + (f_{21}\alpha + f_{22})W_2^{(p+1)}(z-z_{p+1})]\mathrm{e}^{\omega t - \mathrm{i}k_m x}$.

Both representations of the wave field outside and inside the basin are now matched at the irregular interface $\xi(x)$ by satisfying boundary conditions for displacement and traction in the least-squares sense (see Reference 10). This leads to a simultaneous system of equations to be solved for the unknowns A_n in equation

(1) and $B_m^{(1)}$ in equation (9). Once the unknowns A_n and $B_m^{(1)}$ is solved, displacement wave fields in the basin and in the half-space can be computed by means of equations (9) and (1), respectively.

PERFORMANCE OF THE METHOD

The boundary integral scheme used in our method avoids the Rayleigh ansatz error and, therefore, the wave field solution is more accurate than that of Aki–Larner.[4] The solution for layers with velocity gradients, obtained using the confluent hyper-geometric function of Whittaker type combined with Thomson–Haskell propagators, is more precise than that obtained using Thomson–Haskell propagators in which the layers are divided into multiple homogeneous layers. Although a solution can be closely obtained using Thomson–Haskell propagators, our method provides a way to directly obtain a precise solution of the wave propagation in a layer with a velocity gradient. The numerical efficiency of our method depends on the number of the layers, i.e., in the case of a basin with a few thick layers in which velocity gradients exist, our method is more efficient than the Thomson–Haskell method. For the case of a basin with a lot of fine layers, the Thomson–Haskell method is more efficient.

The effects of the artificially determined parameters (such as the location of the sources δ, the distance between the sources ds, and the discrete wave-number step Δk) on the stability of the solutions have not previously been discussed extensively in the literature.

The point source distribution for the boundary integral representation of the wave field outside the basin follows the scheme described by Sanchez–Sesma and Esquivel.[10] In essence, there must be four sources per wavelength to ensure stability. Also, due to the singularity of the Green's function at the interface, the sources are located at a distance δ from the boundary, exterior to the half-space. Inside the basin, the range of the horizontal wave number k should be, strictly speaking, continuous from $-\infty$ to $+\infty$. In practice, due to the limitation of computation, the discretization of the wave number is used to represent the wave field in the basin. The discretization has a wave-number interval Δk together with a truncation between $-k_{\max}$ and $+k_{\max}$ ($k_{\max}$ is chosen so as to keep all the waves with phase velocities larger than a minimum value $c_{\min}$). A semi-circular basins with radius a and a velocity gradient is investigated (Figure 2). The ratio of the sediment density to that of the half-space is 0·6667. The shear velocities at the top V_0 and at the bottom of the basins V_b are a and $2a$, respectively. The shear wave velocities in the half-space of the two basins V_h are $3a$. The non-dimensional frequency of incident wave η is 1. (i.e., $\eta = 2a/\lambda$, λ is the incident wavelength.) The displacements at the stations $x = 0$ and $a/2$ on the surface of the basins are shown in Figure 2 for varying δ and varying ds. The results are unstable for $\delta < 0{\cdot}1a$. Stable results are obtained for $\delta > 0{\cdot}1a$ only if d$s < 0{\cdot}25\lambda$. The criteria to choose parameters δ and ds expressed in terms of half-space velocity V_h and frequency of incident wave f are:

$$\mathrm{d}s < \frac{V_h}{4f} \tag{10}$$

$$\delta > 0{\cdot}1a \tag{11}$$

To investigate the effect of horizontal wave-number interval on the results, we also consider the case of the semi-circular basin used in this section. Figure 3 shows the distribution of the displacement on the surface of the basin in frequency domain, when different values of wave-number interval Δk are used. The normalized frequency η of the incident wave is 1·0 (i.e., $\eta = \omega a/\pi V_h$, V_h is the shear wave velocity in the half-space). Stable results are obtained when Δk is smaller than $2\pi/4a$. According to the relation of wavelength–wave number $k = 2\pi/\lambda$, it seems that if the incident wavelength is larger than the double width of the basin (i.e., $4a$), the effect of the irregularity of the basin on the results is neglectable small. To obtain stable results, the interval of the discrete wave number must be smaller than $2\pi/4a$.

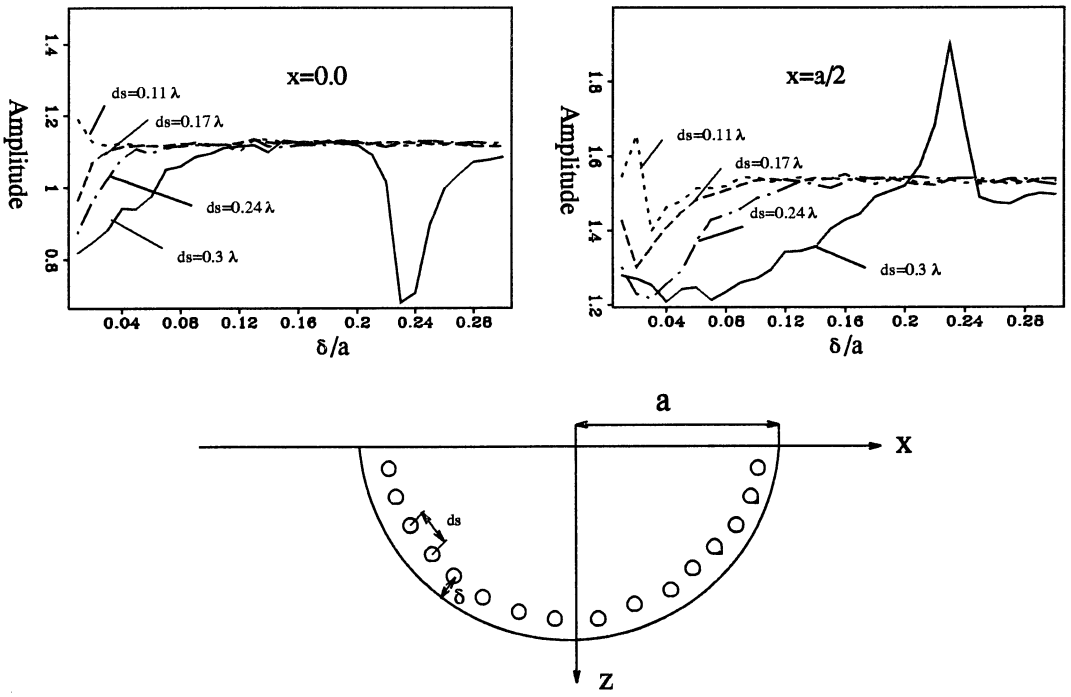

Figure 2. The response displacement at the stations $x = 0$, $a/3$, and $2a/3$ on the surface of a semi-circular basin with a velocity gradient, which changes with the distance between sources ds and the distance of sources off the interface δ. The results become stable if ds is smaller than a quarter of the incident wavelength and if δ is larger than $0{\cdot}1a$

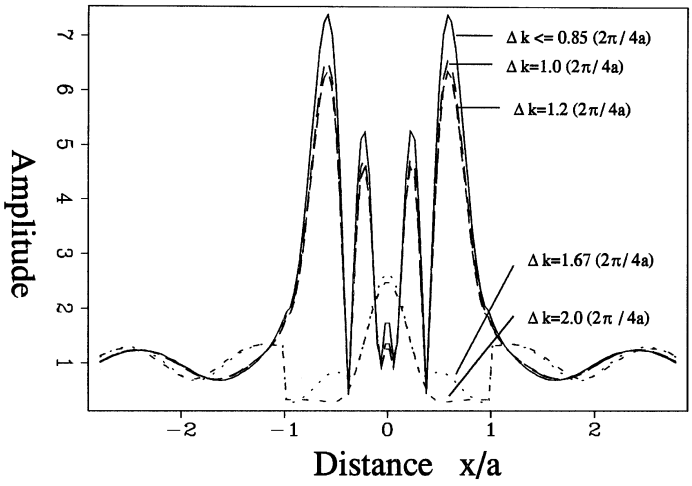

Figure 3. The distribution of surface displacement along the surface of a semi-circular basin with a velocity gradient when the normalized frequency of incident wave $\eta = 1{\cdot}0$. Stable results are obtained when discrete wave-number interval Δk is smaller than $2\pi/4a$

To assess the performance of our method, we compared results with those obtained from Bravo *et al.*'s method[19] and from finite elements.[22] The number of point sources is $N = 48$ and the range of the wave number M in equation (9) is 55. Figure 4 shows the comparisons of the results obtained using our method with those obtained using the above-mentioned methods for normalized frequencies η ranged between $0{\cdot}25$

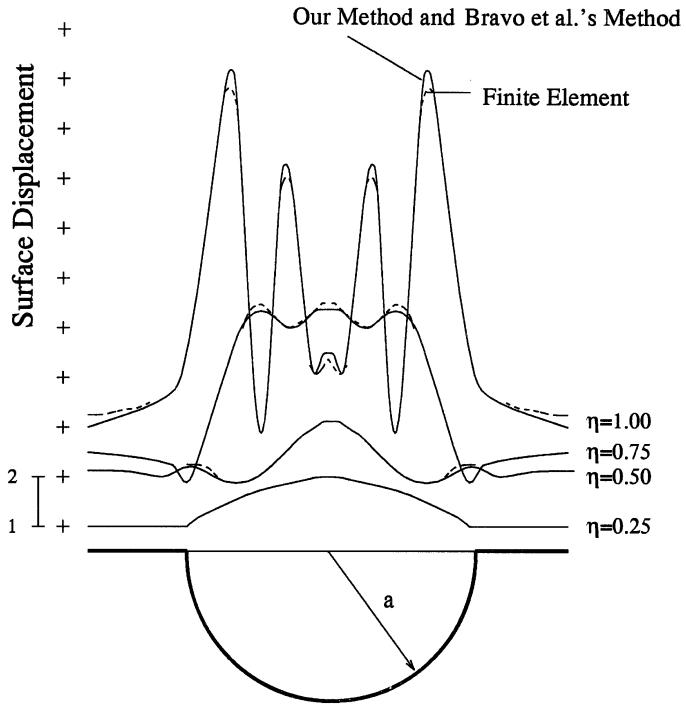

Figure 4. Surface displacement of a semi-circular basin with velocity gradient. The results are compared with those obtained by finite element method and Bravo *et al.*'s method

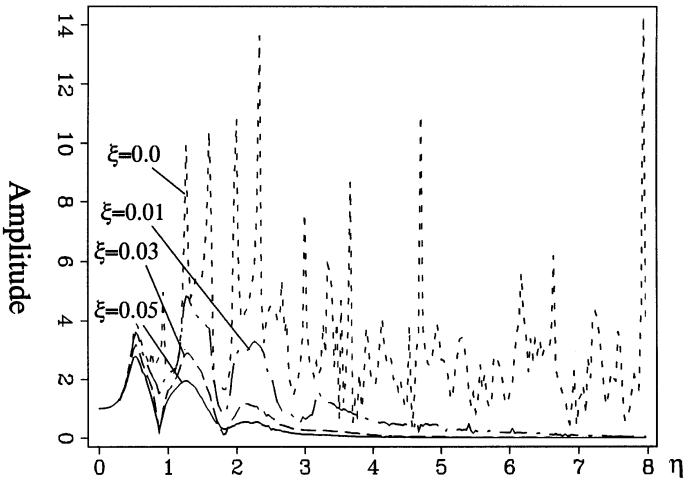

Figure 5. The response amplitude varying normalized frequency at the station $x = 0$ for a semi-circular basin with a velocity gradient for layer damping $\xi = 0{\cdot}0$, $0{\cdot}01$, $0{\cdot}03$, and $0{\cdot}05$

and 1·00. The results are the same as those obtained by Bravo *et al.*'s. The agreement of our results with those obtained by finite elements is excellent.

The damping is introduced by making the shear velocity of the sediments complex:

$$V_s^{\star} = V_s\sqrt{1 + i2\xi\omega/\omega_0} \tag{12}$$

where ξ is damping and V_s is the velocity of the layers in the basin. ω is the angular frequency of incident wave and ω_0 is the fundamental angular frequency of the layers in the basin (The components with frequency $\omega \approx \omega_0$ dominate the response when ξ is very small, i.e., $\xi < 0{\cdot}05$.) The responses at station $x = 0$ in the frequency domain are shown in Figure 5. The results for damping ratio $\xi = 0{\cdot}0$ are dramatically unstable at higher frequencies. When the damping $\xi = 0{\cdot}01$, $0{\cdot}03$, and $0{\cdot}05$ is introduced, the plots become smooth and the stability of the solution is improved, especially, at higher frequencies.

EFFECT OF THE VELOCITY GRADIENTS IN FREQUENCY DOMAIN

We investigated the effects of the velocity gradient in an irregular basin with a sharp interface by computing the responses of two trapezoid-shaped basins: one with a velocity gradient and one with a homogeneous layer. The basin with a velocity gradient has shear velocities of a and $2a$ at the top and at the bottom, respectively. The shear velocity in the half-space is $3a$. The ratio of the density of the sediment to that of the half-space is $0{\cdot}6667$. The damping ratio of the layer is chosen as $0{\cdot}03$. The basin with a homogeneous layer has the same shape, density, and half-space shear velocity. The shear velocity in the homogeneous layer is chosen so that the fundamental frequency equals the fundamental frequency of the layers with a velocity gradient. The equivalent normalized frequency of layer with velocity gradient ε can be calculated by

$$f_0 = 1 \Big/ \int_0^{a/2} \frac{4\,\mathrm{d}z}{(1 + \varepsilon z)V_0} \tag{13}$$

where $a/2$ is the thickness of the sediment and V_0 is the velocity at the top of the basin.

The relation of velocity–frequency for a homogeneous layer with a velocity V_s and a thickness $a/2$ is expressed as

$$f_0 = V_s/2a \tag{14}$$

According to equations (13) and (14), the fundamental frequency of a homogeneous layer is equivalent to that of the layer with velocity gradient when the velocity of the layer is $1{\cdot}49a$. Therefore, the value $1{\cdot}49a$ is chosen as the velocity of the homogeneous layer.

Figure 6 shows the distribution of the displacement along the surface of the two basins under vertical incidence of shear waves with normalized frequencies $\eta = 0{\cdot}75$, $1{\cdot}0$, and $1{\cdot}4$. The results indicate that the amplification of the basin with velocity gradient is generally larger than that of the basin with a homogeneous layer.

Figure 7 is the response at three locations in the two basins for different normalized frequencies η. The incident angles θ are 0 and 45°, respectively. The results show that not only does the basin with velocity gradients have a larger amplification but also the frequencies of the second- and third-order harmonics shift toward lower frequencies. The 1D responses of the sedimentary columns (a homogeneous layer and a layer with velocity gradient) are compared in Figure 8. The response amplitude of the layer with a velocity gradient is larger than that of the homogeneous layer. But the frequencies of the second and third order of harmonics are unchanged. Therefore, the shift in frequencies of the higher-order harmonics must be due to the 2-D effects of the basin.

EFFECT OF THE VELOCITY GRADIENTS IN TIME DOMAIN

A Ricker wavelet with width of $1{\cdot}4$ sec and peak frequency of $0{\cdot}599$ Hz is used as a source time function in our study. The basins considered are the cases of two trapezoid-shaped ones stated in last section. We obtained synthetic seismograms along the surface of the basins by convolving the response in frequency domain with the Fourier transform of the Ricker wavelet. Figure 9 shows the delays of the first arrivals inside the basin due to the lower velocity inside the basins. The response amplitude of the basins with a velocity gradient (a)

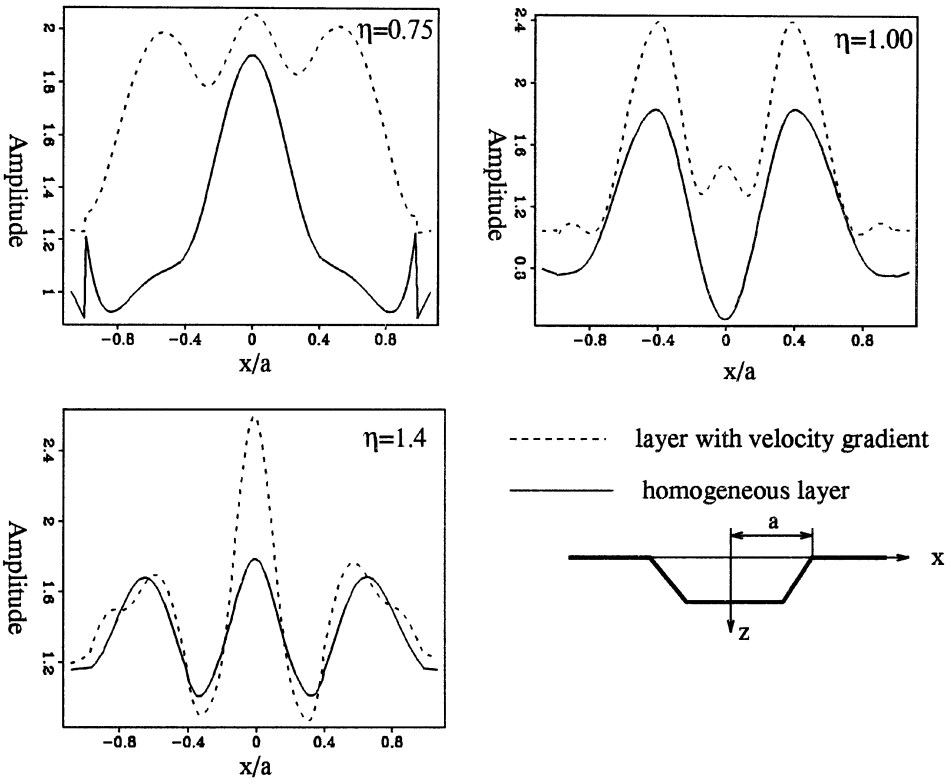

Figure 6. Distribution of the displacement at the surface of a trapezoid-shaped basin with a velocity gradient and a basin with a homogeneous layer for vertical incident waves with normalized frequencies $\eta = 0{\cdot}75$, $1{\cdot}0$, and $1{\cdot}4$

and (b) attenuates more slowly than that of the basin with a homogeneous layer (c) and (d). The waveform of the basins with a velocity gradient is apparently longer than that of the homogeneous basin. This is due to the lower velocity of the upper layer in the basin (which results in lower group and phase velocities) as well as the larger velocity contrast, and therefore more efficient trapping of seismic energy. The contrast results in surface waves propagating forward and backward across the basins yielding larger amplitudes and longer durations. The response of the basins under incidence of plane waves with incident angle of 45° shows more clearly the surface wave transmitting forward and backward across the basins. These are due to the larger velocity contrast across the interface between the sediments and the half-space for the basin with a velocity gradient.

Finally, to investigate the effects of the velocity gradients in more realistic basin, we give two examples of irregular trapezoid-shaped basins for comparison. One has three layers with velocity gradients (Figure 10(a)). While the other has the same geometry of the interface and a homogeneous layer with equivalent frequency of above three layers (Figure 10(b)). As an incident wave, we chose an accelerogram recorded on a rock site in *Waipawa*, New Zealand, in the *Weber* earthquake of February 19, 1990. The earthquake had a local magnitude of 5·9 and the site has an epicentral distance of 61 km. The accelerogram and its normalized acceleration response spectra are shown in Figure 11. The surface response in time domain was calculated by convolving the response in frequency domain with the Fourier transform of incident wave. The accelerogram was sampled at 0·02 sec time intervals and the frequency was between 0 and 10 Hz (The accelerogram is used as an incident wave after the amplitude is multiplied by a factor of 0·5). Figure 12 shows the results of the acceleration response spectra $Sa(T)$ of the basin stations 1, 2 and 3 along the surface of the two basins. The values for the basin with velocity gradients are larger than those of the homogeneous case by approximately

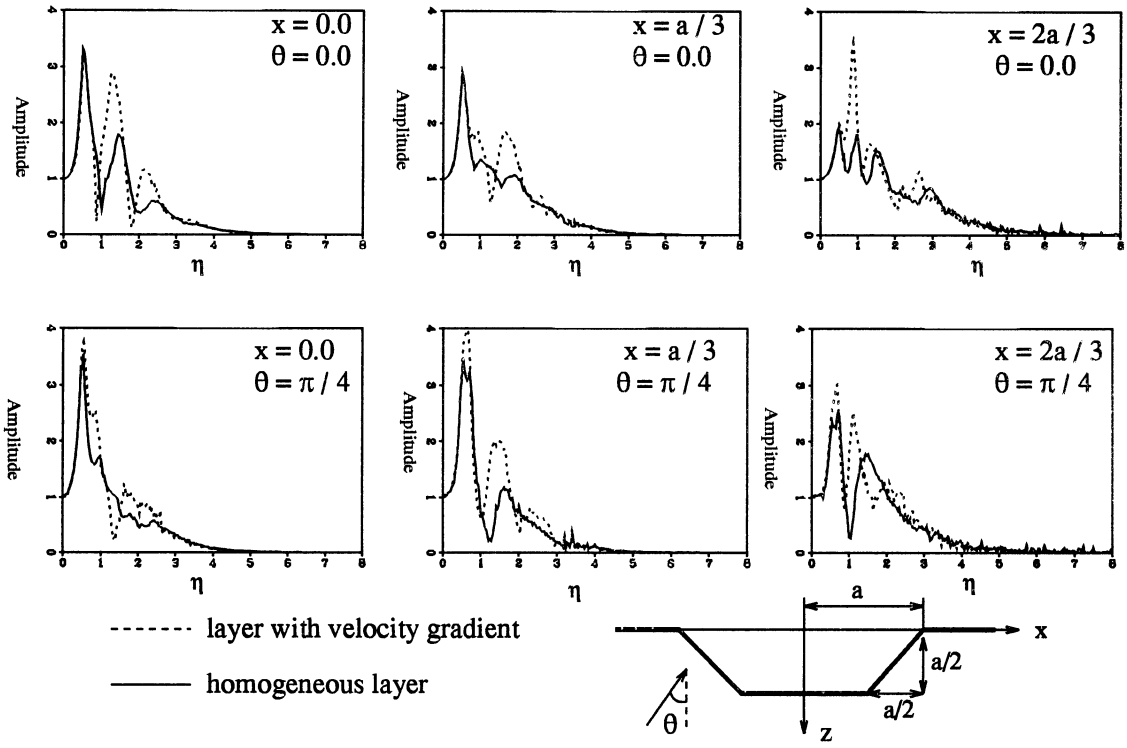

Figure 7. The displacement at the stations $x = 0{\cdot}0$, $a/3$, and $2a/3$ on the surface of a trapezoid-shaped basin with a velocity gradient and a basin with a homogeneous layer for the vertical ($\theta = 0{\cdot}0$) and oblique ($\theta = \pi/4$) incident waves with normalized frequencies η ranged between 0 and 8

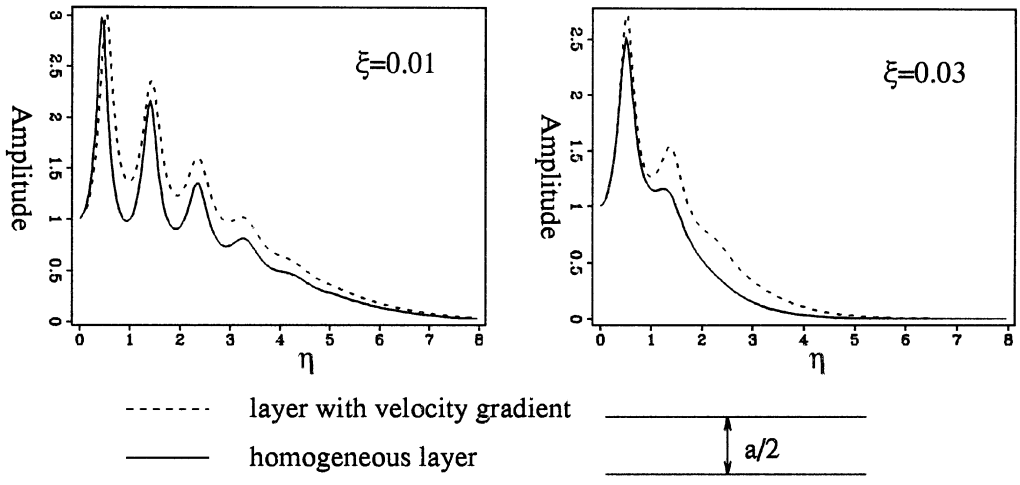

Figure 8. Comparison of surface displacement of a horizontal layer with velocity gradient and that of a homogeneous layer for the incident waves with normalized frequencies ranged between 0 and 8 and for layer damping $\xi = 0{\cdot}01$ and $0{\cdot}03$

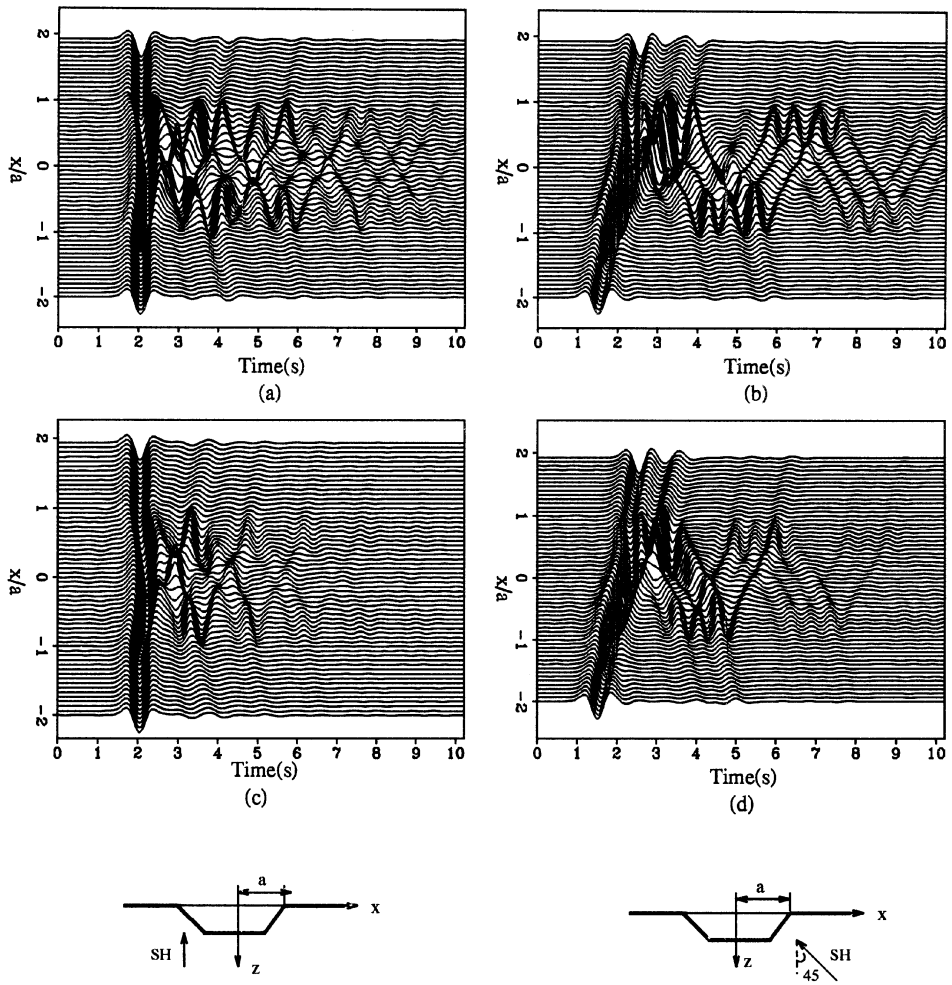

Figure 9. Synthetic seismograms for a trapezoid-shaped basin with velocity gradients (a) and (b) and a basin with a homogeneous layer (c) and (d) vertical and oblique incident waves. The basin with a velocity gradient exhibits larger amplification, longer period of waveform and weak attenuation

10–20 per cent. The shape of the response spectra depends on the position along the surface of basins. The large values of response spectra near the centre of the basins dominate a wide range of periods due to the thickness of layers. Three peak values at periods of about 1·1, 0·7, and 0·5 sec, correspond to the first-, second- and third-order harmonics of the layers. The range of large response spectra becomes narrower with the decrease of layer thickness (see site 3). The response spectra at the edges of the basins (site 1) are nearly the same as that of the incident wave (Figure 11). Comparison of the responses of the two basins shows that the period of the peak values for the basin with velocity gradients shift slightly to longer period than those of the basin with a homogeneous layer. With the layer thickness decreases, the shift effect becomes smaller.

CONCLUSIONS

A boundary-integral method has been presented to study frequency- and time-domain responses of irregular 2-D basins with multiple historical sedimentary layers which exhibit velocity gradients under incident plane shear waves. The procedure combines wave field representations outside the basin and point source distribution

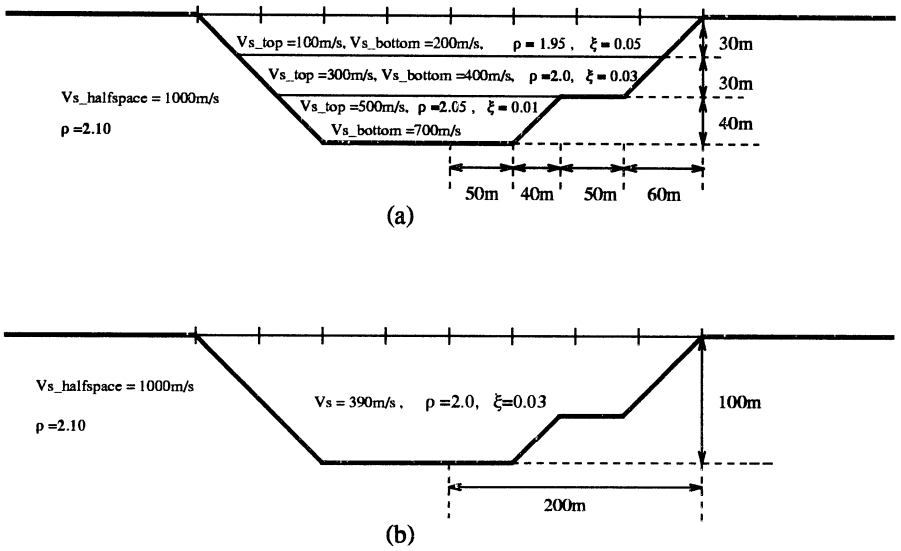

Figure 10. The geometry and parameters of a trapezoid-shaped basin with velocity gradients and a basin with a homogeneous layer. The values of shear velocity V_S, density ρ, and damping ratio ξ used for computation are presented in this figure

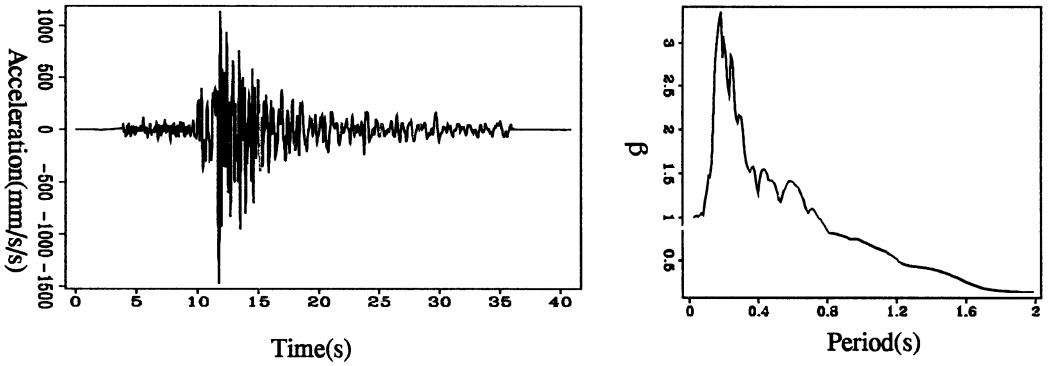

Figure 11. The accelerogram and its normalized response spectrum of seismograms (Component $S41W$) obtained from a rock site of *Waipawa*, New Zealand at an epicenteral distance of 61 km, from the *Weber* earthquake, February 19, 1990. The earthquake had a local magnitude of 5·9

and discrete wave number inside the basin. Propagation through the layers is performed by matrix propagators in which confluent hyper-geometric functions have been incorporated to account for velocity gradients. The testing of the method against other well accepted numerical solutions for a semi-circular inhomogeneous basin shows excellent agreement of results.

Our approach enhances the applications of Bravo *et al.*'s method, particularly when the layers exhibit vertical velocity gradients. The study shows that the results are accurate if the source location off the interface δ is larger than $0{\cdot}1a$ and the distance between sources is smaller than a quarter of an incident wavelength. To get an accurate solution, the wave-number interval Δk must be small enough so that the incident wavelength is larger than the double width of the basin.

The responses of basins with sharp interfaces and several horizontal deposits are computed in the frequency domain and time domain. Following conclusions are obtained: (1) the amplification of the basin with velocity gradients is larger than that of a basin with homogeneous layers; (2) the frequencies of the second- and

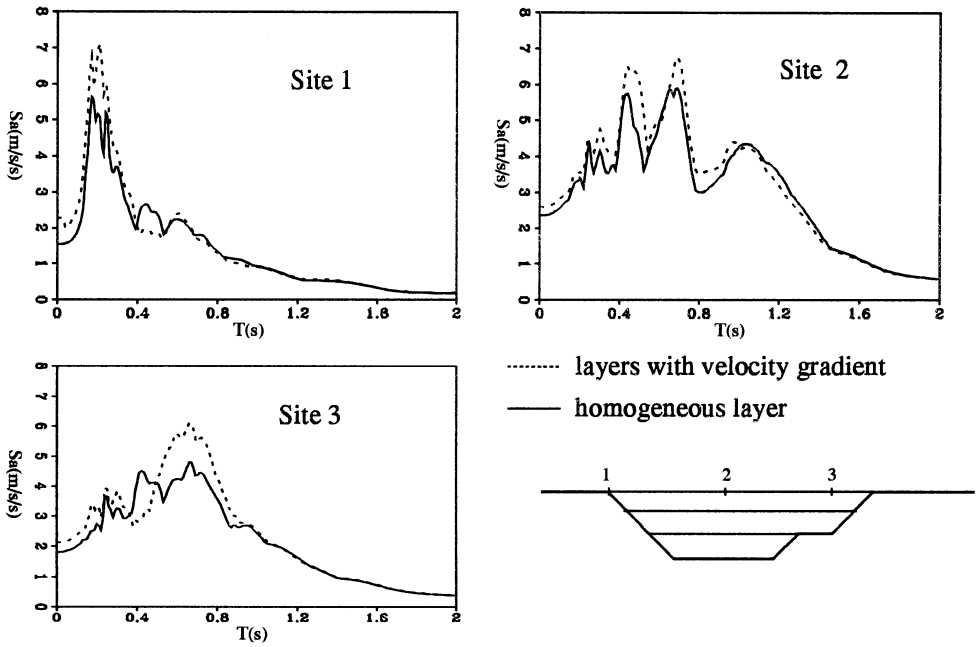

Figure 12. Comparison of acceleration spectra $S_a(T)$ at stations on the the surface of a basin with velocity gradients and a basin with a homogeneous layer illustrated in Figure 10

third-order harmonics for the basin with gradients are lower than those of the basin with homogeneous layers; (3) the response amplitude of the basin with velocity gradients attenuates more slowly than when layers are homogeneous. Our method and results should be of significance in earthquake engineering or seismic microzonation studies.

ACKNOWLEDGEMENTS

The authors would like to express his gratitude to J. X. Zhao, R. Robinson, R. Cuthbertson and the anonymous reviewers for their valuable suggestion of modifying the manuscript. This work was supported by the Institute of Geological and Nuclear Sciences and by the Joint New Zealand-Sino Scientific Research Program.

REFERENCES

1. K. Aki, 'Local site effects on strong ground motion', in J. L. Von Thun (ed.), *Earthquake Engineering and Soil Dynamics II: Recent Advanced in Ground Motion Evaluation*, Geotechnical Special Publication, No. 20, *Am. Soc. Civil Engr.*, New York, 1988, pp. 103–155.
2. M. D. Trifunac, 'Surface motion of a semi-cylindrical alluvial valley for incident plane SH waves', *Bull. Seism. Soc. Am.* **72**, 1167–1183 (1971).
3. K. Aki, and K. L. Larner, 'Surface motion of a layered medium having an irregular interface due to incident plane SH waves', *J. Geophys. Res.* **75**, 933–954 (1970).
4. M. Bouchon, 'A simple complete numerical solution to the problem of diffraction of SH waves by an irregular surface', *J. Acoust. Soc. Am.* **77**, 1–5 (1985).
5. P.-Y. Bard, and M. Bouchon, 'The seismic response of sediment-filled valleys. Part 1. The case of incident SH waves', *Bull. Seism. Soc. Am.* **70**, 1263–1286 (1980).
6. P.-Y. Bard, and B. E. Tucker, 'Ridge and tunnel effects: comparing observations with theory', *Bull. Seism. Soc. Am.* **75**, 905–922 (1985).
7. P.-Y. Bard, and J. C. Gariel, 'The seismic response of two-dimensional sedimental deposits with large vertical velocity gradients', *Bull. Seism. Soc. Am.* **76**, 343–366 (1986).
8. H. L. Wong, M. D. Trifunac and B. Westermo, 'Effects of surface and subsurface irregularities on the amplitudes of monochromatic waves', *Bull. Seism. Soc. Am.* **67**, 353–368 (1977).

9. F. J. Sanchez-Sesma, and E. Rosenblueth, 'Ground motion at canyons of arbitrary shape under incident plane SH waves', *Earthquake Engng. Struct. Dyn.* **7**, 441–450 (1979).
10. F. J. Sanchez-Sesma, and J. A. Esquivel, 'Ground motion on alluvial valleys under incident plane SH waves', *Bull. Seism. Soc. Am.* **69**, 1107–1120 (1979).
11. T. K. Mossessian, and M. Dravinski, 'Application of a hybrid method for scattering of P, SV, and Rayleigh waves by near-surface irregularities', *Bull. Seism. Soc. Am.* **77**, 1784–1803 (1987).
12. H. Kawase, 'Time domain response of a semi-circular canyon for incident SV, P, and Rayleigh waves calculated by discrete wavenumber boundary element method', *Bull. Seism. Soc. Am.* **78**, 1415–1432 (1988).
13. H. A. Petersen, F. J. Sanchez-Sesma and M. Campillo, 'Three-dimensional scattering by two-dimensional topographies', *Bull. Seism. Soc. Am.* **84**, 1169–1183 (1994).
14. J. E. Luco, and F. C. P. De Barros, 'Three-dimensional response of a layered cylindrical valley embedded in a layered half-space', *Earthquake Engng. Struct. Dyn.* **24**, 109–125 (1995).
15. M. Kawano, S. Matsuda, K. Toyoda and J. Yamada, 'Seismic response of three-dimensional alluvial deposit with irregularities for incident wave motion from a point source', *Bull. Seism. Soc. Am.* **84**, 1801–1814 (1994).
16. D. L. Karabalis, and D. E. Beskos, 'Dynamics response of 3D rigid surface foundation by time domain boundary element method', *Earthquake Engng. Struct. Dyn.* **12**, 73–93 (1984).
17. M. Bouchon, and O. Coutant, 'Calculation of synthetic seismograms in a laterally varying medium by the boundary element discrete wavenumber method', *Earthquake Engng. Struct. Dyn.* **84**, 1869–1881 (1994).
18. Y. Hisada, K. Aki and T. Teng, '3-D simulations of surface wave propagation in the kanto sedimentary basin, Japan. Part 2. Application of the surface wave beam', *Bull. Seism. Soc. Am.* **83**, 1700–1720 (1993).
19. M. A. Bravo, F. J. Sanchez-Sesma and F. J. Chavez-Garcia, 'Ground motion on stratified alluvial deposits for incident SH waves', *Bull. Seism. Soc. Am.* **78**, 436–450 (1988).
20. E. T. Whittaker, and G. N. Wastson, *A Course of Modern Analysis,* 4th edn, Cambridge University Press, Cambridge, England, 1952.
21. M. Ewing, W. S. Jardesky and F. Press, *Elastic Waves in Layered Media*, McGraw-Hill, New York, 1957.
22. R. Benites, and K. Aki, 'Ground motion at mountains and sedimentary basins with vertical seismic velocity gradient', *Geophys. J. Int.* **116**, 95–118 (1994).
23. F. J. Sanchez-Sesma, and F. Luzon, 'Seismic response of three-dimensional alluvial valleys for incident P, S, and Rayleigh waves', *Bull. Seism. Soc. Am.* **85**, 269–284 (1995).

